



Influence of Fe on Microstructure and Mechanical Properties in P-doped Ni–Cr–Fe Alloys

Xin-Tong Lian^{1,2} · Wen-Ru Sun¹ · Xin Xin¹ · Fang Liu¹ · Dan-Dan Zheng¹

Received: 3 July 2018 / Revised: 2 August 2018 / Published online: 19 September 2018
© The Chinese Society for Metals and Springer-Verlag GmbH Germany, part of Springer Nature 2018

Abstract

The influence of Fe on the microstructure and mechanical properties of P-doped Ni–Cr–Fe alloys has been investigated. Results showed that increasing Fe content refined the dendrite microstructure and enhanced the solubility of P in as-cast alloys. The change of microhardness in different dendrite regions was attributed to the segregation of P atoms in solid solution state, which had strengthening effects. Increasing Fe contents from 15.2 to 60.7 wt% reduced the yield strength and tensile strength but had little influence on the elongation of alloys. The stress rupture life of alloys after heat treatment decreased with the increment of Fe contents, and the failure fracture modes transferred from transgranular to intergranular fracture mode. The change of fracture modes was due to the weakness of grain boundaries caused by the increment of Fe. In addition, the precipitation of $M_{23}C_6$ was believed to be related to the segregation of P toward grain boundaries, which led to the fluctuation of carbon and chromium atoms near the grain boundaries in alloys with low Fe contents. Consequently, the increment of Fe decreased the strength of matrix and changed the existence of P atoms and the precipitates at grain boundaries.

Keywords Fe · P · Segregation · Precipitate · Mechanical properties

1 Introduction

Nickel-based superalloys have emerged as the materials for high-temperature applications, due to their significant resistance to fatigue and creep conditions [1–3]. In this kind of alloys, more than ten alloying elements are added, making them consequently among the most complex materials. Certain superalloys, such as IN718 and IN706, containing significant proportion of Fe, are often referred as Ni–Fe superalloys [2]. Elements including Ni, Fe and Cr refer to the formation of austenitic γ , and C, B and P tend to segregate toward grain boundaries with different atomic sizes from Ni [4, 5].

P as an alloy element has been drawn attention in recent years with moderate addition can improve the mechanical properties in specific alloys. For example, the increase of P promoted the precipitation of M_3B_2 and $M_{23}C_6$ and then prolonged the stress rupture life of GH761 [6, 7]. In addition, P in the IN718 led to the strengthening of the alloy matrix [8, 9]. However, the addition of P was reported to weaken the tensile strength, but improve the impact energy of Ni–Cr alloys [10]. For IN783, the interfacial cohesion strength in heavily P-doped alloy was weakened and the stress rupture life was shortened [11]. Obviously, the beneficial effect of P on mechanical properties is selective and depends on alloy systems.

It is known that GH761 and IN718 alloys are Ni–Cr–Fe-based alloys, while IN783 and Waspalloy are Ni–Fe-based and Ni–Cr-based alloys. It may be related to the difference of compositions in alloys such as the scale of Fe content and Ni content. Ge et al. adjusted the content of Fe from 0 to 25 wt% to study the change of microstructure and properties in Ni–Cr–Mo–Al–Ti-based alloys [12, 13]. It was found that the number of MC increased, while $M_{23}C_6$ was prohibited with the increment of Fe. The stress rupture life also decreased, but the tensile strength changed

Available online at <http://link.springer.com/journal/40195>

✉ Wen-Ru Sun
wrsun@imr.ac.cn

¹ Institute of Metal Research, Chinese Academy of Sciences, Shenyang 110016, China

² School of Materials Science and Engineering, Shanghai University, Shanghai 200444, China

slightly. However, the influence of Fe on the action of P in the matrix is still controversial, which needs further study [14].

Based on the previous study, the addition of alloy elements may cause the precipitates toward grain boundaries, leading to solid solution strengthening of matrix, which makes the microstructure complicated. In this work, four P-doped alloys with various Fe contents are designed according to the ready-made superalloys such as IN718, IN706 and GH761 alloys. Because the Fe content of these alloys varies from 22.0 to 48.5 wt%, the model alloys are designed to contain large composition range from 15.0 to 60.0 wt% to study the effect of Fe more clearly. The strengthening elements such as Al, Ti and Nb are removed to eliminate their influence. The work mainly focuses on the effects of Fe on microstructure and mechanical properties, especially the effects on the segregation and solid solubility of P atoms in the matrix of Ni–Cr–Fe alloys.

2 Experimental

The alloys used in this study were prepared in a vacuum induction melting furnace using high purity raw materials under the same conditions to get the as-cast ingots. The chemical compositions of ingots are listed in Table 1. Then, the ingots were forged into bars of 40 mm square section and rolled into round bars of 12 mm in diameter. The as-rolled alloys were heat-treated at 1100 °C for 20 min and then followed by water quenching. The samples were extracted from the same place in the bars and subsequently etched in a solution of (5 g CuCl₂ + 100 ml HCl + 100 ml C₂H₅OH). Metallographic characterization was performed by a Axiovert 200 MAT optical microscope (OM) and a JEOL 6340 scanning electron microscope (SEM) equipped with Oxford INCA energy-dispersive spectrometry (EDS). The precipitates were identified by a JEM 2010 transmission electron microscope (TEM). The element distribution and precipitates were identified by a Shimadzu Seisakusho 1610 electron probe microanalyzer (EPMA) and EDS attached on SEM.

LECO Microstructure Tester LM247AT was used to examine the change of Vickers microhardness in different

areas of as-cast alloys. Tensile test specimens with 5 mm in gauge diameter and 25 mm in gauge length were tested at 650 °C. The strain rate stayed at $1.5 \times 10^{-4} \text{ s}^{-1}$ before the sample was yielded and turned to $1.0 \times 10^{-3} \text{ s}^{-1}$ after the sample was yielded. The stress rupture properties of the alloys were measured at 650 °C under a stress of 150 MPa. The fracture surfaces were examined, and the rupture samples were cut into two halves along the load axis to reveal the initiation and propagation of cracks by OM and SEM.

3 Results

3.1 As-cast Microstructure, Segregation and Microhardness

Noticeable effects of Fe on the microstructure of as-cast ingots are shown in Fig. 1. The dendrite cores in alloy 1 appeared in a bright color, while the interdendritic areas appeared in a dark color. The primary dendrite arm space (PDAS) was wide, and the average secondary dendrite arm space (SDAS) was about 120 μm (Fig. 1a). In alloy 2, the dendrite was refined obviously by increasing Fe content. The PDAS and SDAS both decreased, and SDAS reduced to a scope of about 70 μm (Fig. 1b). In alloy 3 and alloy 4, increasing Fe content was favorable to form short and narrow primary dendrites as well as thinner PDASs and SDASs and fine dendrite structure (Fig. 1c, d). No precipitates were observed in the dendrite cores or the interdendritic regions.

In order to evaluate the segregation degree, the composition of dendrite cores and interdendritic areas was measured and the partition coefficient, *k*, (defined as the ratio of dendrite core to interdendritic area composition) is listed in Table 2. Ni, Fe and Cr tended to be distributed uniformly in the matrix because the *k* values in different areas were all about 1. However, the segregation of P was influenced significantly by Fe content. In alloy 1 and alloy 2, the contents of P in interdendritic areas were 0.079 wt% and 0.080 wt%, respectively, while no P content was detected in dendrite cores, which indicated that P was extremely depleted in dendrite cores and enriched in interdendrite regions. However, the concentration of P in dendrite cores was high than that in interdendrite regions in alloy 3 and alloy 4. The contents of P in dendrite cores were 0.035 wt% and 0.044 wt%, respectively, but no P was found in the interdendritic areas. It indicated that P segregated toward dendrite cores by increasing Fe content.

The effect of Fe on Vickers microhardness in different dendrite areas of as-cast alloys is shown in Fig. 2. The hardness in interdendrite regions was higher than that in dendrite cores of alloy 1 and alloy 2. However, in alloy 3

Table 1 Chemical compositions of different Ni–Cr–Fe alloys (wt%)

Alloy no.	Fe	P	Cr	C	Ni
1	15.2	0.025	17.17	0.039	Bal.
2	30.5	0.025	17.11	0.040	Bal.
3	45.1	0.024	17.14	0.044	Bal.
4	60.7	0.026	17.17	0.041	Bal.

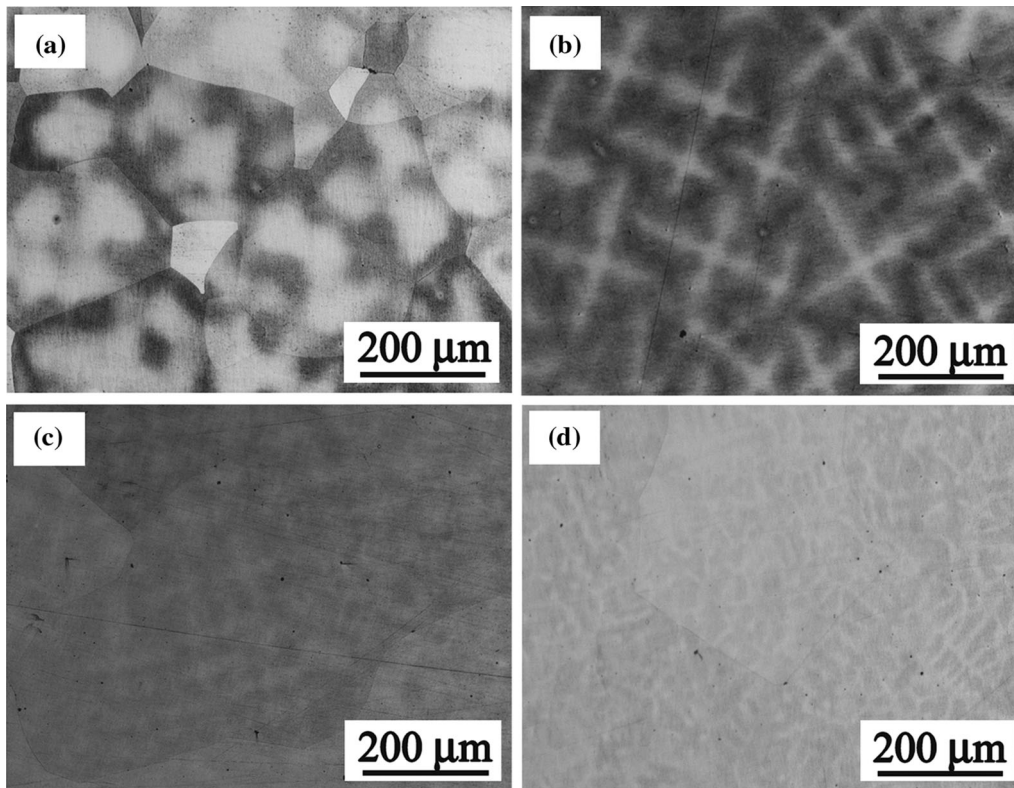


Fig. 1 Dendrite structure of as-cast Ni–Cr–Fe alloys: a alloy 1; b alloy 2; c alloy 3; d alloy 4

Table 2 Distribution and partition coefficients of elements in different alloys by EPMA (wt%)

Alloy no.	Region	Ni	Fe	Cr	P
1	Dendrite core	67.94	15.27	16.79	–
	Interdendritic area	66.46	15.10	18.36	0.079
2	Dendrite core	1.02	1.01	0.91	–
	Interdendritic area	51.51	31.82	16.67	–
3	Dendrite core	51.30	30.78	17.84	0.080
	Interdendritic area	1.00	1.03	0.93	–
4	Dendrite core	37.80	44.68	17.49	0.035
	Interdendritic area	36.71	46.43	16.86	–
4	Dendrite core	1.03	0.96	1.04	–
	Interdendritic area	21.67	60.27	18.02	0.044
		20.23	62.73	17.04	–
		1.07	0.96	1.06	–

and alloy 4, the hardness in interdendrite regions was reduced and lower than that in dendrite cores.

3.2 As-heat-Treated Microstructure

In order to eliminate the influence of grain size on mechanical properties, the as-rolled alloys were heat-

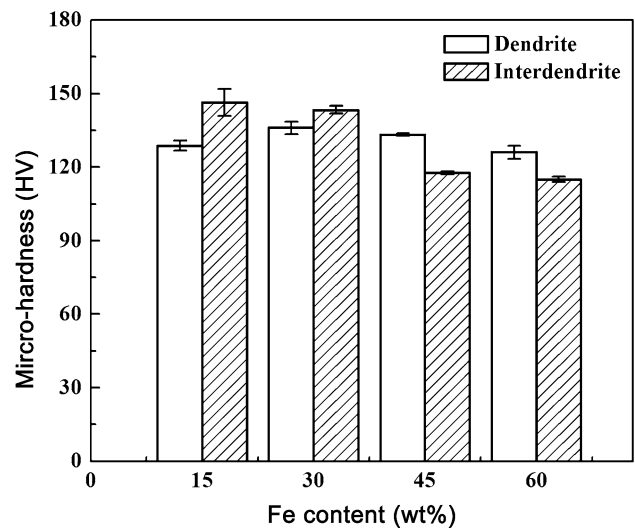


Fig. 2 Vickers microhardness of different alloys in dendrite and interdendrite regions

treated and the typical microstructures are shown in Fig. 3. The average grain size of these four alloys was all about 250 μm regardless of the Fe contents. No precipitate was observed at grain boundaries. The morphologies of the microstructures in different alloys had no obvious difference.

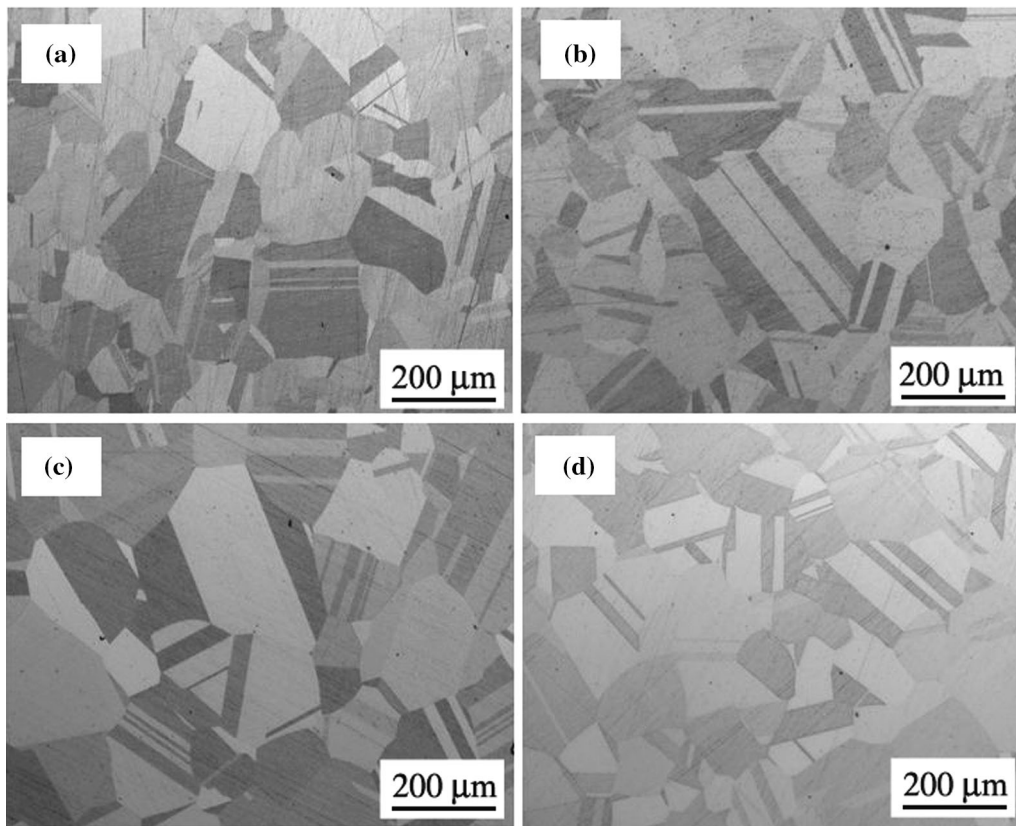


Fig. 3 Microstructures of as-rolled alloys after heat treatment: **a** alloy 1; **b** alloy 2; **c** alloy 3; **d** alloy 4

3.3 Tensile Properties

The tensile properties of as-heat-treated alloys tested at 650 °C are illustrated in Fig. 4. With the increase of Fe from 15.2 to 60.7 wt%, the yield strength of samples decreased from 302 to 183 MPa and the tensile strength declined from 416 to 324 MPa. However, the elongation of

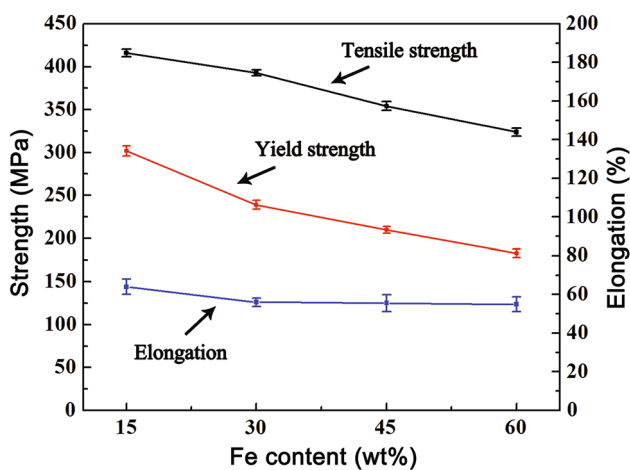


Fig. 4 Effects of Fe content on tensile properties of alloys

alloys decreased slightly and then remained stable with the increment of Fe contents.

The typical SEM images of tensile fracture surfaces are shown in Fig. 5. In alloy 1, the fracture surface was flat and smooth, characterized by small size dimples (Fig. 5a, e). With the increase of Fe contents, the areas of shear lips and fiber regions were enlarged and the dimples were bigger and bigger. At this point, the tensile fracture partially occurred, as evidenced by some apparent necking, especially in alloy 4 (Fig. 5d, h). Although the fracture surfaces of these four alloys were all dominated by transgranular fracture characteristics, different morphologies of dimples and fracture regions existed on the surfaces. The transgranular fracture mode indicated that the strength of grain boundaries was higher than that of grain interior during tensile tests. It could be deduced that grain interior strength controlled the tensile fracture process mainly. It was obvious that the increase of Fe contents lowered the strength of matrix. Larger fractions of shear lips and fiber regions and bigger dimples also supported this result.

3.4 Stress Rupture Properties

The stress rupture properties of heat-treated alloys tested at 650 °C and 150 MPa are illustrated in Fig. 6. The stress

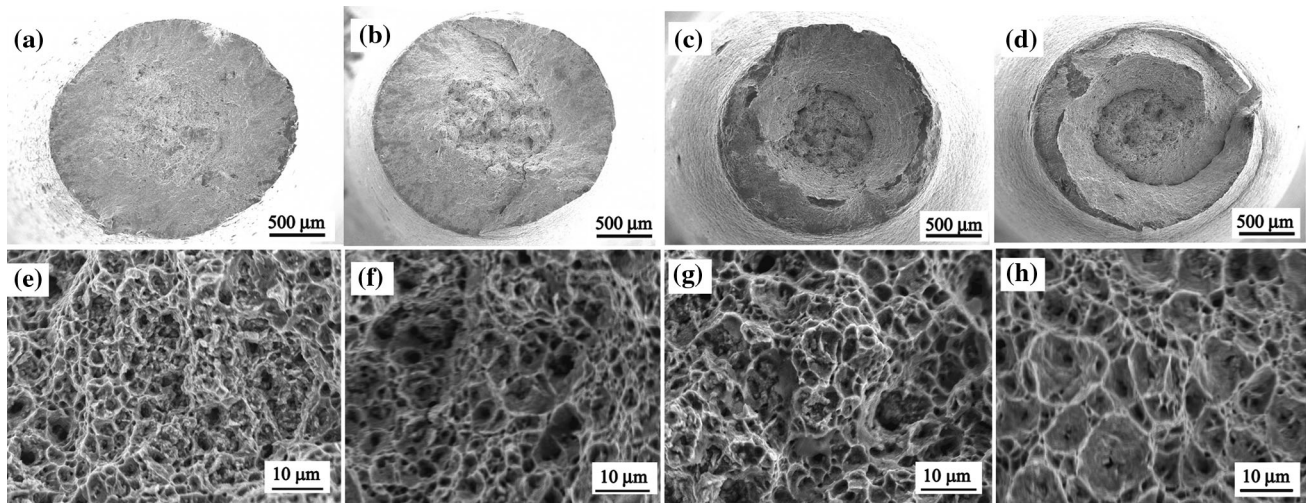


Fig. 5 Morphologies of fracture surfaces after tensile tests for alloy 1 **a, e**, alloy 2 **b, f**, alloy 3 **c, g**, alloy 4 **d, h** at low **a–d**, high **e–h** magnification

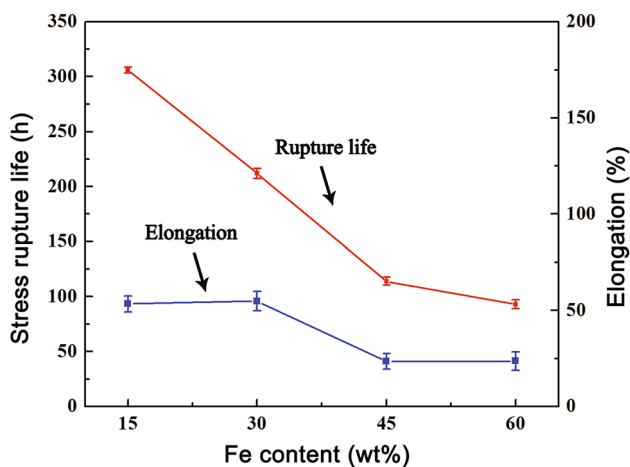


Fig. 6 Effects of Fe content on stress rupture properties of alloys

rupture life decreased dramatically from 306 to 93 h with increasing Fe ranged from 15.2 to 60.7 wt%. Furthermore, the rupture ductility of the alloys was deeply influenced by increasing Fe contents. The elongations of alloy 1 and alloy 2 were 53.4% and 54.8%, while those of alloy 3 and alloy 4 were reduced to 23.5% and 23.6%, respectively.

The fracture surfaces of the stress rupture samples were examined, as shown in Fig. 7. The morphology of stress rupture surface was quite different from that of tensile rupture surface. In alloy 1, minor intergranular fracture zone was identified at the edge of the surface, while the rest part was transgranular fracture zone (Fig. 7a) with a large amount of dimples at higher magnification by SEM (Fig. 7e). In alloy 2, the area of intergranular fracture was enlarged (Fig. 7b) and mixed fracture mode was dominated (Fig. 7f). The entire surfaces were covered by intergranular cracks, and typical intergranular failure mode was

dominated in alloy 3 and alloy 4 (Fig. 7c, d). It should be noted that the grain boundaries in alloy 4 were much wider than that in alloy 3, which demonstrates that grain boundaries were weakened with the increase of Fe contents (Fig. 7g, h). Therefore, the fracture modes transferred from transgranular fracture mode to intergranular fracture mode during stress rupture tests.

In order to study the initiation of the cracks, longitudinal section microstructure along the loading direction was investigated. In alloy 1 and alloy 2, the grains were elongated along the stress axis with obvious plastic deformation. A large number of secondary crack cavitations were observed at the triple points of grain boundaries, but the cracks could hardly propagate along grain boundaries. Although cracks were initiated on grain boundaries, the cracks grew through interior grains, which indicated that the strength of grain boundary was higher than that of intergranular strength (Fig. 8a, b). However, many broad intergranular cracks were found in alloy 3 and alloy 4 and the cracks propagated along grain boundaries accompanied with cavities interlinking (Fig. 8c, d). It demonstrated that the stress rupture process was mainly controlled by the strength of grain boundaries rather than the grain interior strength.

Further analysis of the results showed the reason why the fracture mode changed. Taken alloy 1 and alloy 3 for example, the cracks in alloy 1 were formed in the junctions of grain boundaries as indicated by the arrows, but they could not propagate along grain boundaries (Fig. 9a). Magnified by the rectangular part as shown in Fig. 9a, a kind of precipitates was observed along grain boundaries in alloy 1 and the precipitate hindered the intergranular crack propagation (Fig. 9c). In alloy 3, the cracks were initiated from grain boundaries and then grew along grain

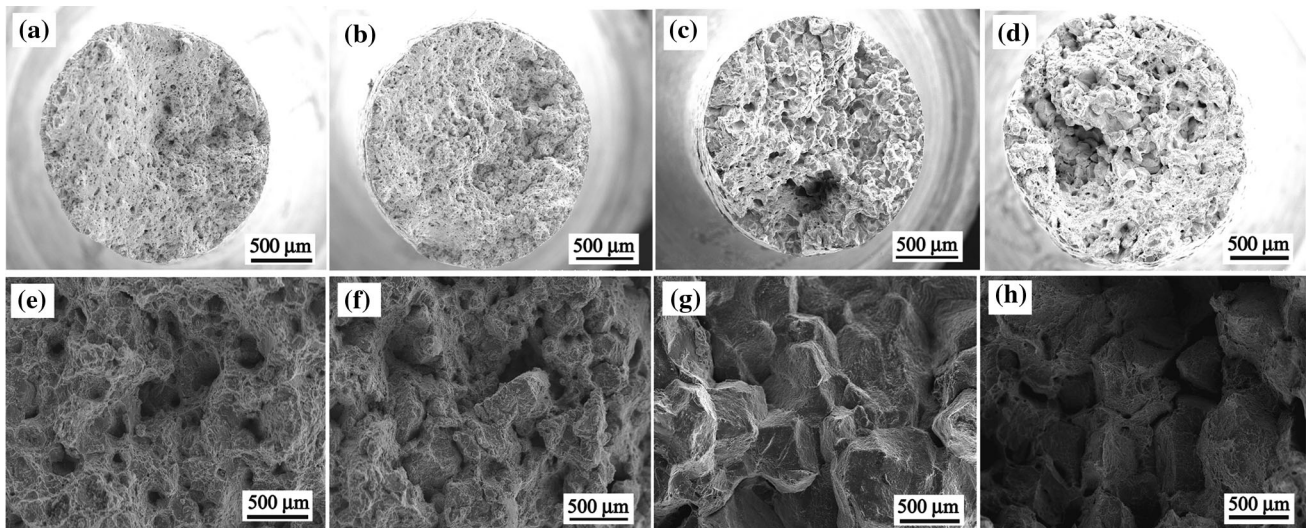


Fig. 7 Morphologies of fracture surfaces after stress test for alloy 1 **a, e**, alloy 2 **b, f**, alloy 3 **c, g**, alloy 4 **d, h** at low **a–d**, high **e–h** magnification

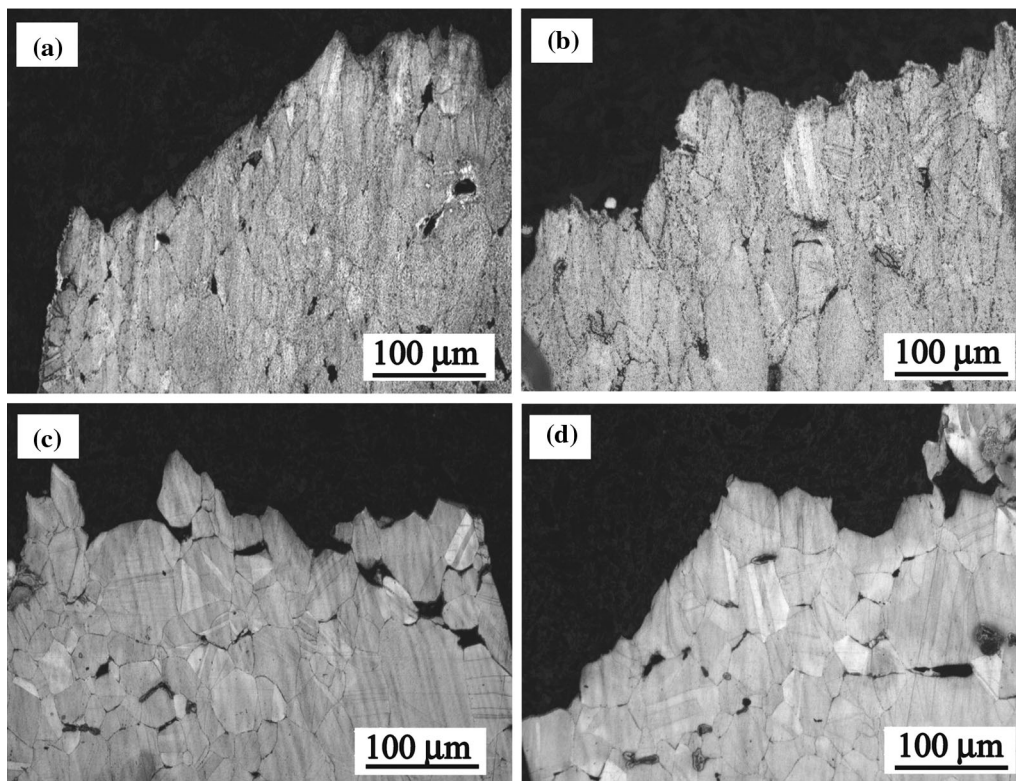


Fig. 8 Longitudinal microstructures of stress-ruptured alloys at 650 °C and 150 MPa: **a** alloy 1; **b** alloy 2; **c** alloy 3; **d** alloy 4

boundaries (Fig. 9b). It was clear that no precipitate was found in alloy 3 (Fig. 9d). Based on the previous study [15], the granular grain boundary precipitate was determined to be $M_{23}C_6$ with the average size of about 300–500 nm according to the weak diffraction patterns and EDS analysis (Fig. 9e, f). It should be noted that some P was enriched in carbides.

4 Discussion

4.1 Effects of Fe on As-cast Microstructure and P Segregation

The metal may remain in the liquid state below its solid–liquid equilibrium temperature which is called supercooled liquid during a cooling process. Once the grains are

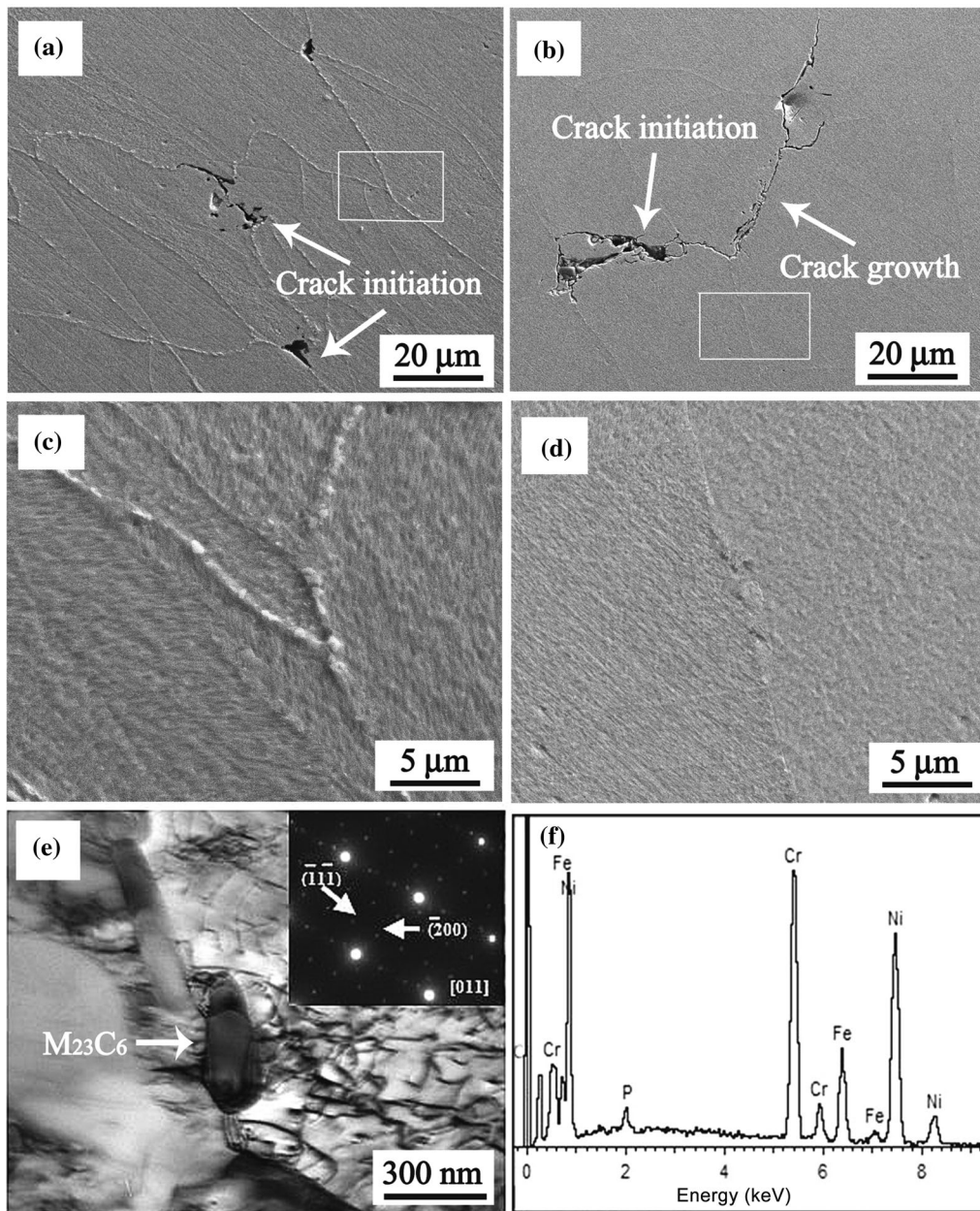


Fig. 9 Morphologies of grain boundaries in stress rupture of **a, c** alloy 1, **b, d** alloy 3 at **a, b** low, **c, d** high magnification, **e** TEM image, **f** EDS analysis of $M_{23}C_6$ in alloy 1

nucleated in supercooled liquid, the growth of grains will not be stable and dendrite microstructures are formed, depending on several factors especially the degree of constitutional supercooling [16–18]. It is related to the high and low liquidus temperature of the alloys and crystallization temperature of interval. It can be seen that from the phase diagram of Ni–Cr–Fe systems, the width of mushy zone becomes narrow with the increase of Fe content, which indicates that the degree of supercooling is reduced [19]. The growth of dendrites is inhibited, and PDASs and SDASs are obviously reduced with the decrease of

supercooling. Therefore, increasing Fe content refines the dendrite microstructure.

P is concentrated in interdendrite regions in the alloys with low Fe contents (15.2 wt% and 30.5 wt%), while P segregates toward dendrite cores in alloys with high Fe content (45.1 wt% and 60.7 wt%) according to Table 2. It is known that the dendrite cores are preferentially nucleated during solidification and the interdendritic regions are formed in the final stage. In the alloys with low Fe contents, oversaturated P atoms are released into the remained metal liquid in the areas of interdendrite due to the low

solid solubility of P in the matrix. When the cooling progress is finished, a large number of P atoms will eventually be stored in the interdendritic areas. In alloys with high contents, the solubility of P in the matrix increases significantly, thus accommodating more P atoms in the dendrite cores. So the level of P content in interdendritic regions decreases significantly. The change of P levels from interdendrite regions to dendrite cores indicates that the solubility of P in the matrix is increased. Therefore, the solid solubility of P in alloys has been improved by increasing Fe. In addition, it is known that the decrease of element segregation is also beneficial for refining dendrites. The increase of Fe decreases the segregation of elements because the solubility of P in Fe is higher than that in nickel, which indicates that the alloy matrix can contain more P atoms. It demonstrates once again that the increment of Fe refines the dendrite microstructure.

The segregation of P in different areas in the as-cast microstructure has directly influenced the Vickers microhardness. The hardness in interdendrite regions is higher than those in dendrite cores of alloy 1 and alloy 2, while that in interdendrite regions is reduced and lower than those in dendrite cores in alloy 3 and alloy 4. The variation of hardness is probably attributed to the solution strengthening effect of P because nickel, Fe, chromium and carbon have no obvious segregation in different regions. It is reported that P can change the mismatch lattice and thus increase lattice distortion [20]. Therefore, the high concentration of P atoms in solid may result in the increase of lattice distortion and thus enhances the microhardness.

4.2 Effect of Fe on Precipitates

After tensile tests, no precipitate is found in these four alloys. However, some intergranular $M_{23}C_6$ carbides are precipitated along grain boundaries in alloys with low Fe contents, while no $M_{23}C_6$ is precipitated in alloys with high Fe contents during stress rupture tests. It is known that the nucleation of $M_{23}C_6$ precipitation is closely related to the atom diffusion [21, 22]. C, Cr and P atoms are enriched in $M_{23}C_6$ carbides as shown in Fig. 9f. Under the dual functions of stress field and temperature field, C and Cr atoms are driven by diffusion activation energy, diffusing from matrix toward grain boundaries. It is because that grain boundaries provide the fast channels for element transfer. Although the solubility of P in the matrix of superalloys is always low, the solubility of P will be increased with the enlargement of Fe percentage in matrix because the solubility of P in Fe is larger than that in Ni [23]. P segregation toward grain boundaries has been widely proved [17, 24]. Therefore, low Fe content promotes C, Fe and P atoms to segregate toward grain boundaries and the atoms will occupy the vacancies in the grain boundaries. The

segregation of elements on grain boundaries facilitates the nucleation of intergranular $M_{23}C_6$. The reason why $M_{23}C_6$ contains P is probably that the P atoms are oversaturated both on grain boundaries and in the matrix of interior grains, and excess P atoms diffuse into $M_{23}C_6$ in alloys with low Fe contents. The growth of intergranular $M_{23}C_6$ carbides continues to consume C and P atoms in matrix and grain boundaries. The change of Fe contents causes the fluctuation of carbon, chromium and P atoms toward grain boundaries. In alloys with high Fe contents, the solid solubility of matrix for C, Cr and P atoms is all enhanced. The energy produced by segregation of elements toward grain boundaries is not enough to cause the nucleation of $M_{23}C_6$ even in longtime stress rupture tests. In tensile tests, the phenomenon of no precipitate along grain boundaries is probably attributed to that atom diffusion is not sufficient in a short period of time. It is logical to deduce that the test duration and element diffusion caused by the change of Fe content are the main factors for the precipitation of intergranular $M_{23}C_6$.

4.3 Mechanical Role of Fe and P

As results mentioned above, the tensile strength and stress rupture life of these four alloys all decrease with the enhancement of Fe contents. It is obvious that the proportionate improvement in the scale of Fe in the matrix reduces the strength of alloys. However, different failure mechanisms have been determined although tensile tests and stress rupture tests are both conducted at the temperature of 650 °C. The main differences for tensile tests and stress rupture tests are tensile strain rate and applied stress level. In tensile tests, the tensile strain rate stays at $1.5 \times 10^{-4} \text{ s}^{-1}$ before the sample is yielded and turns to $1.0 \times 10^{-3} \text{ s}^{-1}$ after the sample is yielded, which is much higher than that of stress rupture tests. Combined with the transgranular fracture modes of these four alloys in tensile tests, it is sure that the strength of grain boundaries is higher than that of grain interior, but the fracture modes change in stress rupture tests. Alloy 1 (15.2 wt% Fe) possesses the longest stress rupture life which is mainly controlled by the transgranular failure mode. Although the intergranular fracture zone at the periphery of the fracture surface is believed to be the initial failure zone, the cracks propagate through the grain interior, which indicates that the grain boundary strength is still higher than interior strength. In alloy 2 (30.5 wt% Fe), the area of intergranular failure is enlarged and the fracture surface is dominated by mixed failure modes including transgranular failure and some minor intergranular failure. In alloy 3 (45.1 wt% Fe) and alloy 4 (60.7 wt% Fe), the cracks are more inclined to initiate from and propagate along grain boundaries, thus leading a typical transgranular failure mode. In addition, a

large number of secondary cracks in alloy 4 indicate that the binding force of grain boundaries has been weakened seriously. In crack initiation stage, it is believed that oxide cracking can result in crack initiation, which shortens the stress rupture life [25, 26]. Therefore, oxygen atoms may diffuse along grain boundaries and bring in the grain boundary oxidation because the stress rupture samples are exposed to high-temperature field and stress field for a long time. But this needs further investigation.

The precipitation of intergranular $M_{23}C_6$ in the alloys with low Fe contents can also enhance the grain boundary strength due to the slip of dislocations prevented by grain boundaries. It is known that granular precipitates at grain boundaries can strengthen the grain boundaries [27, 28]. The cracks are hindered by particle $M_{23}C_6$ at grain boundaries and are obliged to propagate through the grains, although cavities are found in the triple junctions of grain boundaries. Therefore, the increment of Fe decreases the strength of alloy matrix and inhibits grain boundary precipitates, which causes crack propagating along the grain boundaries, leading to the decrease of tensile strength and stress rupture life.

5 Conclusion

Increasing Fe content in P-doped Ni–Cr–Fe alloy refined the dendrite structure and improved the solubility of P in the matrix. The existence of P atoms in the dendrites had strengthening effect and increased the microhardness. The increase of Fe inhibited the precipitation of intergranular $M_{23}C_6$, which was believed to be related to the fluctuation of C, Cr and P atoms toward grain boundaries. The increase of Fe decreased the yield and tensile strength and had no obvious effect on elongation of the samples in tensile tests. The fracture modes of tensile samples were mainly controlled by transgranular fracture modes. Although the stress rupture life was also decreased by increasing Fe content, the failure fracture mode transferred from transgranular fracture mode to intergranular fracture mode. It was because that increasing contents of Fe led to the weakness of grain boundaries when the samples were exposed to high-temperature field and stress field for a long time.

References

- [1] G. Smith, L. Shormaker, *Adv. Mater. Process.* **162**, 23 (2004)
- [2] C.T. Sims, N.S. Stoloff, W.C. Hagel, *Superalloys II: High-Temperature Materials for Aerospace and Industrial Power* (Wiley, New York, 1987), pp. 2–3
- [3] D.Z. Fan, D. Wang, C. Liu, G. Zhang, J. Shen, L.H. Lou, J. Zhang, *Acta Metall. Sin. (Engl. Lett.)* **30**, 878 (2017)
- [4] R.C. Reed, *The Superalloys Fundamentals and Applications* (Cambridge University Press, Cambridge, 2006), pp. 24–35
- [5] D.D. Shen, *Acta Metall. Sin. (Engl. Lett.)* **17**, 639 (2004)
- [6] S.L. Yang, W.R. Sun, J.X. Wang, Z.M. Ge, S.R. Guo, Z.Q. Hu, *J. Mater. Sci. Technol.* **27**, 539 (2011)
- [7] W.R. Sun, S.R. Guo, D.Z. Lu, Z.Q. Hu, *Metall. Mater. Trans. A* **28**, 649 (1997)
- [8] W.R. Sun, S.R. Guo, J.H. Lee, N.K. Park, Y.S. Yoo, S.J. Choe, Z.Q. Hu, *Mater. Sci. Eng. A* **247**, 173 (1998)
- [9] M.Q. Wang, J.H. Du, Q. Deng, Z.L. Tian, J. Zhu, *Mater. Sci. Eng. A* **626**, 382 (2015)
- [10] W.D. Cao, R.L. Kennedy, in *Superalloys*, ed. by R.D. Kissinger (TMS, Warrendale, 1996), p. 597
- [11] L.X. Yu, Y.R. Sun, W.R. Sun, X.F. Sun, S.R. Guo, Z.Q. Hu, *Mater. Sci. Eng. A* **527**, 911 (1998)
- [12] Z.Y. Ge, R.Z. Ye, J.G. Sun, H. Wang, L.Y. Yang, *J. Univ. Sci. Technol. B* **2**, 11 (1983)
- [13] Z.Y. Ge, R.Z. Ye, J.G. Sun, *J. Univ. Sci. Technol. B* **4**, 43 (1983)
- [14] J.J. Ge, S.Q. Yuan, G. Yi, G.C. Zhang, Y.Z. Li, J. Chen, Z.G. Sun, X.L. Zhu, H.D. Liu, *Ordinance Mater. Sci. Eng.* **32**(2), 107 (2009)
- [15] H.R. Pruppacher, *Pure Appl. Geophys.* **104**, 623 (1973)
- [16] G.V. Raynor, V.G. Rivlin, *Bull. Alloy Phase Diagr.* **2**(1), 90 (1981)
- [17] X. Xiao, H.Q. Zhao, C.S. Wang, Y.A. Guo, J.T. Guo, L.Z. Zhou, *Acta Metall. Sin.* **49**, 421 (2013). (in Chinese)
- [18] Q.Z. Chen, C.N. Jones, D.M. Knowles, *Mater. Sci. Eng. A* **385**, 417 (2004)
- [19] R.M. Wang, Y.G. Song, Y.F. Han, *J. Alloys Compd.* **311**, 64 (2000)
- [20] S. Zhang, X. Xin, L.X. Yu, A.W. Zhang, W.R. Sun, X.F. Sun, *Metall. Mater. Trans. A* **47**, 4094 (2016)
- [21] T. Alam, P.J. Felfer, M. Chaturvedi, L.T. Stephenson, M.R. Kilburn, J.M. Cairney, *Metall. Mater. Trans. A* **43**, 2187 (2012)
- [22] W.M. Gui, H.Y. Zhang, H.B. Long, T. Jin, X.F. Sun, Q. Zheng, *Acta Metall. Sin. (Engl. Lett.)* **31**, 27 (2018)
- [23] A.V. Bromley, P.H. Parker, *Metall. Technol.* **11**, 421 (1984)
- [24] J.X. Dong, M.C. Zhang, X.S. Xie, R.G. Thompson, *Mater. Sci. Eng. A* **328**, 8 (2001)
- [25] S. Cruchley, H.Y. Li, H.E. Evans, P. Bowen, D.J. Child, M.C. Hardy, *Int. J. Fatigue* **81**, 266 (2015)
- [26] Y.B. Hu, L. Zhang, C.Q. Cheng, P.T. Zhao, G.P. Guo, J. Zhao, *Acta Metall. Sin. (Engl. Lett.)* **30**, 857 (2017)
- [27] Q.Z. Chen, C.N. Jones, D.M. Knowles, *Mater. Sci. Eng. A* **385**, 414 (2004)
- [28] R.M. Wang, Y.G. Song, Y.F. Han, *J. Alloys Compd.* **311**, 63 (2000)